Guidance to students

You should read the article, methods and extended data. Answer these basic questions to check yourself:

– Where is the source of entangled pairs in the actual scheme of this experiment? Where is the Bell analyser?

– Exactly which optical element prepares the polarization state to be teleported? How is this state changed from one to another?

– How do the ground station and satellite keep their telescopes precisely pointed at each other, while the satellite moves across the sky quite fast? What equipment is used to maintain the pointing?

– How many quantum states in total have been teleported in this entire experiment and what time has this taken?

– In the theoretical teleportation protocol, Alice should send to Bob the result of her Bell state measurement (two classical bits), and Bob perform one of the four unitary transformations on the received photon. Is this actually implemented in this experiment?

We will discuss the following three questions *in the classroom:*

– For an attempt of state teleportation to succeed, how many detectors in the experiment (both on the ground and the satellite) have to click simultaneously?

– Per an attempt to teleport the state, what is the probability of it to succeed in the basic (theoretical) teleportation protocol? What is the probability to succeed in this experiment? What practical factors make the latter much lower than the former?

– Why do we use four photons in each teleportation attempt? In the basic teleportation protocol, only three photons are involved. Why do we ever bother to detect here the fourth "trigger" photon?

LETTER

doi:10.1038/nature23675

Ground-to-satellite quantum teleportation

Ji-Gang Ren[1,2], Ping Xu[1,2], Hai-Lin Yong[1,2], Liang Zhang[2,3], Sheng-Kai Liao[1,2], Juan Yin[1,2], Wei-Yue Liu[1,2], Wen-Qi Cai[1,2], Meng Yang[1,2], Li Li[1,2], Kui-Xing Yang[1,2], Xuan Han[1,2], Yong-Qiang Yao[4], Ji Li[5], Hai-Yan Wu[5], Song Wan[6], Lei Liu[6], Ding-Quan Liu[3], Yao-Wu Kuang[3], Zhi-Ping He[3], Peng Shang[1,2], Cheng Guo[1,2], Ru-Hua Zheng[7], Kai Tian[8], Zhen-Cai Zhu[6], Nai-Le Liu[1,2], Chao-Yang Lu[1,2], Rong Shu[2,3], Yu-Ao Chen[1,2], Cheng-Zhi Peng[1,2], Jian-Yu Wang[2,3] & Jian-Wei Pan[1,2]

An arbitrary unknown quantum state cannot be measured precisely or replicated perfectly[1]. However, quantum teleportation enables unknown quantum states to be transferred reliably from one object to another over long distances[2], without physical travelling of the object itself. Long-distance teleportation is a fundamental element of protocols such as large-scale quantum networks[3,4] and distributed quantum computation[5,6]. But the distances over which transmission was achieved in previous teleportation experiments, which used optical fibres and terrestrial free-space channels[7–12], were limited to about 100 kilometres, owing to the photon loss of these channels. To realize a global-scale 'quantum internet'[13] the range of quantum teleportation needs to be greatly extended. A promising way of doing so involves using satellite platforms and space-based links, which can connect two remote points on Earth with greatly reduced channel loss because most of the propagation path of the photons is in empty space. Here we report quantum teleportation of independent single-photon qubits from a ground observatory to a low-Earth-orbit satellite, through an uplink channel, over distances of up to 1,400 kilometres. To optimize the efficiency of the link and to counter the atmospheric turbulence in the uplink, we use a compact ultra-bright source of entangled photons, a narrow beam divergence and high-bandwidth and high-accuracy acquiring, pointing and tracking. We demonstrate successful quantum teleportation of six input states in mutually unbiased bases with an average fidelity of 0.80 ± 0.01, well above the optimal state-estimation fidelity on a single copy of a qubit (the classical limit)[14]. Our demonstration of a ground-to-satellite uplink for reliable and ultra-long-distance quantum teleportation is an essential step towards a global-scale quantum internet.

In our experiment, the quantum state to be teleported is the polarization of a single photon: $|\chi\rangle_1 = \alpha|H\rangle_1 + \beta|V\rangle_1$, where α and β are unknown complex numbers satisfying $|\alpha|^2 + |\beta|^2 = 1$, and $|H\rangle$ and $|V\rangle$ denote the horizontal and vertical polarization states, respectively, which can be used to encode the basic logic states $|0\rangle$ and $|1\rangle$ for a quantum bit (qubit), and the subscript '1' labels the photon. Such a single qubit is generated at an observatory ground station in Ngari, Tibet (32° 19′ 33.07″ N, 80° 1′ 34.18″ E, altitude of 5,047 m), with the aim of teleporting it to the Micius satellite that was launched from China on 16 August 2016 to an altitude of about 500 km. The satellite flies along a Sun-synchronous orbit; that is, it passes over any given point on Earth's surface at the same local solar time (00:00).

Quantum teleportation[2] relies on using both a classical channel and a quantum channel (entanglement), shared between the two communicating parties; we refer to these parties as Ngari and Micius. The entangled state of a pair of photons can be written as $|\phi^+\rangle_{23} = (|H\rangle_2|H\rangle_3 + |V\rangle_2|V\rangle_3)/\sqrt{2}$, one of the four maximally entangled two-qubit Bell states (here photon 2 is at Ngari and photon 3 is at the satellite). Ngari performs a joint measurement on the photon that is to be teleported (photon 1) and one of the photons from the entangled pair (photon 2), projecting them into one of the four Bell states. When the Bell-state measurement yields $|\phi^+\rangle_{12} = (|H\rangle_1|H\rangle_2 + |V\rangle_1|V\rangle_2)/\sqrt{2}$, the other photon from the entangled pair (photon 3) carries exactly the desired state. If another Bell state, $|\phi^-\rangle_{12} = (|H\rangle_1|H\rangle_2 - |V\rangle_1|V\rangle_2)/\sqrt{2}$, is detected, then the state of photon 3 is equivalent to the original state of photon 1, up to a unitary π phase shift in the data post-processing.

The experimental realization of quantum teleportation of an independent single photon necessitates the simultaneous creation of two entangled photon pairs[15] and high-visibility quantum interference between them[7]. The multi-photon coincidence count rate is several orders of magnitude lower than in typical single- or two-photon experiments. Owing to the complexity of the multi-photon set-up for space-to-ground-scale quantum teleportation, we choose the uplink configuration (Fig. 1a) in which the transmitter (Ngari) is placed in the ground station and the receiver (Micius) is in the satellite. To maximize the count rate in the experiment, we prepare compact and ultra-bright four-photon sources (Fig. 1b). Ultraviolet femtosecond pulses (with a central wavelength of 390 nm, pulse width of 160 fs and repetition rate of 80 MHz) from a mode-locked Ti:sapphire laser pass through two bismuth borate (BiBO) crystals to generate two pairs of photons. The first pair is generated via collinear spontaneous parametric down-conversion (SPDC), whereby one of the photons is detected as a trigger to herald the presence of photon 1 (count rate of $5.7 \times 10^5\,s^{-1}$), whose state is to be teleported. Using a half-wave plate (HWP) and a quarter-wave plate (QWP), the initial polarization state of photon 1 can be arbitrarily prepared. The second BiBO crystal was aligned for non-collinear SPDC[16] and prepared in the frequency-uncorrelated polarization-entangled state $|\phi^+\rangle_{23}$, with a count rate of $1 \times 10^6\,s^{-1}$ and a fidelity of 0.933 measured on the ground (see Methods).

To realize the Bell-state measurement, photons 1 and 2 are then overlapped on a polarizing beam splitter (PBS), which transmits H and reflects V polarization. After the PBS, we select the events that correspond to each output detecting one photon, which is possible only if the two photons have the same polarization—$|H\rangle_1|H\rangle_2$ or $|V\rangle_1|V\rangle_2$—thus projecting the wave function into a subspace of $|\phi^\pm\rangle_{12} = (|H\rangle_1|H\rangle_2 \pm |V\rangle_1|V\rangle_2)/\sqrt{2}$. Finally, by measuring the photons in the $(|H\rangle \pm |V\rangle)/\sqrt{2}$ bases at the outputs of the PBS, we can distinguish between $|\phi^+\rangle_{12}$ and $|\phi^-\rangle_{12}$ (ref. 17). After the Bell-state measurement, the final four-photon count rate measured on the ground is $4{,}080\,s^{-1}$. To achieve high stability, the four-photon interferometry system is integrated into a compact platform with dimensions of 460 mm × 510 mm × 100 mm and a weight of less than 20 kg (see Methods and Extended Data Fig. 1). The variation in the four-photon

[1]Department of Modern Physics and Hefei National Laboratory for Physical Sciences at the Microscale, University of Science and Technology of China, Hefei 230026, China. [2]Chinese Academy of Sciences (CAS) Center for Excellence and Synergetic Innovation Center in Quantum Information and Quantum Physics, University of Science and Technology of China, Shanghai 201315, China. [3]Key Laboratory of Space Active Opto-Electronic Technology, Shanghai Institute of Technical Physics, Chinese Academy of Sciences, Shanghai 200083, China. [4]National Astronomical Observatories, Chinese Academy of Sciences, Beijing 100012, China. [5]Nanjing Astronomical Instruments Company Limited, Chinese Academy of Sciences, Nanjing 210042, China. [6]Shanghai Engineering Center for Microsatellites, Shanghai 201203, China. [7]Beijing Institute of Tracking and Telecommunication Technology, Beijing 100094, China. [8]State Key Laboratory of Astronautic Dynamics, Xi'an Satellite Control Center, Xi'an 710061, China.

© 2017 Macmillan Publishers Limited, part of Springer Nature. All rights reserved.

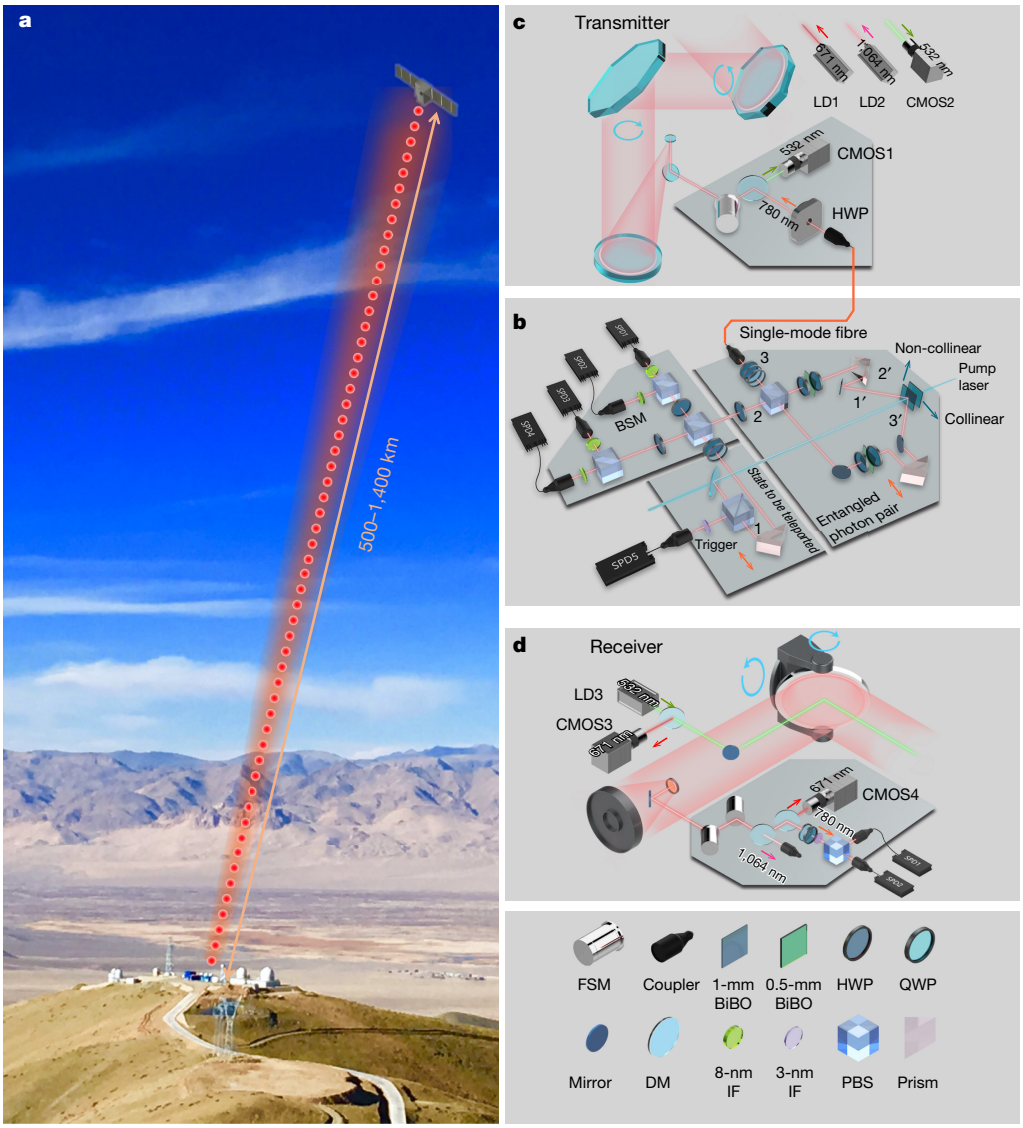

Figure 1 | Overview of the set-up for ground-to-satellite quantum teleportation of a single photon over distances of up to 1,400 km. **a**, A schematic of the satellite is overlaid on a photograph of the Ngari ground station in Tibet. The separation between the satellite and the ground station varies from about 500 km to 1,400 km during quantum teleportation. **b**, The compact multi-photon set-up for teleportation at the ground station. The 390-nm pulsed laser passes through two closely mounted BiBO crystals, producing two photon pairs through collinear SPDC (the two photons are in the same spatial mode 1′) and non-collinear SPDC (the two photons are separated in spatial modes 2′ and 3′). Photons 2′ and 3′ are then superposed on a PBS to disentangle their frequency information from their polarization information for the preparation of entangled photons (labelled '2' and '3') with high brightness and high fidelity[16]. The two photons from collinear SPDC in spatial mode 1′ are first separated from the pump beam using a dichroic mirror (DM) and then separated by a PBS; the state of the transmitted photon (labelled '1') is teleported, whereas the reflected photon serves as a trigger. Photons 1 and 2 are then combined on another PBS for Bell-state measurement (BSM). Narrowband 3-nm and 8-nm filters are used to erase the frequency correlation of the down-converted photons. The teleported photon (photon 1) is collected by a single-mode fibre and guided to the transmitting antenna (shown in **c**). To increase the overall four-photon count rate, a second four-photon module (not shown) with the same design and using the same pump laser is prepared and used for multiplexing (see Methods).SPD1–SPD5, single-photon detectors. **c**, The transmitting antenna. A faster-steering mirror (FSM) and two-axis gimbal mirrors are used for fine and coarse tracking. The dichroic mirror is used to separate the signal and beacon light. The top right inset illustrates a 671-nm continuous-wave laser and a 1,064-nm pulsed laser with a repetition rate of 10 kHz shooting from the ground to the satellite for APT and time synchronization, respectively. A CMOS camera is used to image the beacon laser from the satellite. **d**, The receiver on the satellite. A similar APT system to that at the ground station is implemented. A polarization analyser consisting of a QWP, a HWP and a PBS is used, followed by two single-photon detectors (SPD1 and SPD2).CMOS1–CMOS4, cameras; LD1–LD3, laser diodes; IF, interference filter.

count rate is observed to be less than 10% for the two weeks during which the set-up was mounted in the Ngari observatory station. Using the same pump laser, a second multi-photon module with the same design is built in sequence, which increases the four-photon count rate to 8,210 s^{-1} by multiplexing (see Methods).

Compared to our downlink experiment[18], a substantial challenge for the uplink channel is that the atmospheric turbulence occurs at the beginning of the transmission path, which causes beam wandering and broadening that increases the amount of spreading of the travelling beams. We designed a transmitting telescope with narrow divergence, and developed a high-bandwidth and high-precision acquiring, pointing and tracking (APT) system to optimize the uplink efficiency. The multi-stage APT system consists of coarse and fine tracking, with a tracking error of about 3 μrad (see Methods and Extended Data Fig. 2). The single photons that are teleported from a single-mode fibre are transmitted through a 130-mm-diameter off-axis reflecting telescope

© 2017 Macmillan Publishers Limited, part of Springer Nature. All rights reserved.

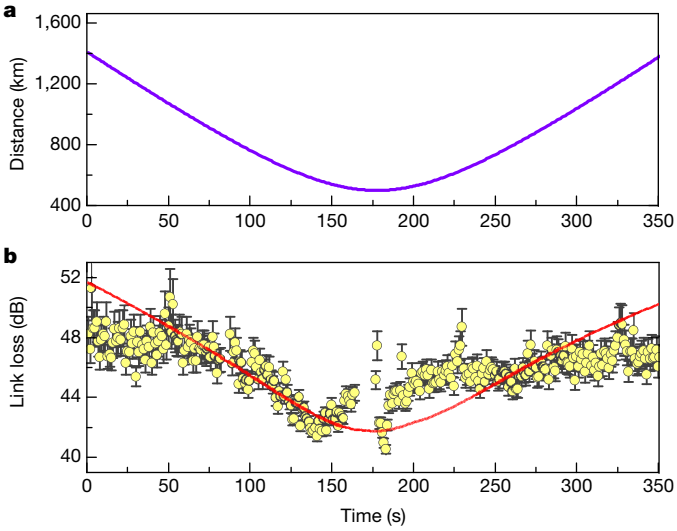

Figure 2 | Distance from the ground station to the orbiting satellite and the measured attenuation during one orbit. a, The trajectory of the Micius satellite measured from the Ngari ground station over one orbit with a duration of 350 s. **b**, The measured ground-to-satellite channel loss using a strong reference laser as a function of time. The highest loss is about 52 dB at a distance of 1,400 km (when the satellite is at an angle of 14.5°). The lowest loss is about 41 dB at a distance of around 500 km (when the satellite is at an angle of 76.0°). The red curve is a model (see Methods) that considers the effect of distance variation. Error bars show one standard error, calculated from Poissonian counting statistics. Owing to the structure of the altazimuth telescope at the ground station, the rotation speed of the optical transmitter has to be increased as a function of the increasing altitude angle of the satellite. When the satellite reaches the top altitude angle, the speed that is required can be very large and beyond the ability of the APT system. The tracking accuracy is therefore reduced with increasing rotational speed, leading to larger measured channel attenuation when the satellite is closer to the ground station. As a result, the trend in the data appears more compressed than the model. This model does not fully capture all of the features of the measured data of channel loss.

(Fig. 1c) and received by a 300-mm-diameter telescope installed in the satellite (Fig. 1d). The locally tested beam divergence angle of the transmitting antenna is approximately 14 ± 1 μrad (Extended Data Fig. 2c), measured with a long-focal-length collimator on the ground. The atmospheric seeing in Ngari is about 5 μrad, which in principle increases the divergence angle to around 15 μrad. In our experiment, we couple the photons that are emitted from stars into a single-mode fibre and measure the intensity distribution as a function of the fine-tracking scanning angle. The effective divergence angle that is estimated from the measured field-of-view (FOV) of the intensity distribution (Extended Data Fig. 2d) is 22 ± 3 μrad; many additional factors can make the scan result of the FOV larger, including the mismatch between the size of the diffraction spot and the radius of the core of the fibre, the altitude angle of star, the precision of the tracking and changes in the atmospheric environment. Finally, the beam divergence as a result of the rapid flight of the satellite is tested by sending an attenuated laser (about 20 billion photons per second) to the satellite, which receives and measures the beam by varying the fine-tracking angle. The intensity pattern that we obtained is elliptical, with an equivalent divergence of 24–35 μrad.

In Fig. 2 we show a time trace of that channel attenuation measured during one orbit of the satellite passing over the Ngari station. The physical distance between the ground station and the satellite varies from a maximum of 1,400 km (at an altitude angle of 14.5°, the starting point of our measurement) to a minimum of 500 km (at the highest altitude angle of 76.0°, when the satellite passes directly over the ground station); as a result, the channel loss of the uplink varies from 52 dB to 41 dB, respectively, as measured using a high-intensity reference laser.

After passing through the uplink, the teleported photon is detected by two fibre-coupled silicon avalanche photodiodes (Fig. 1d). Before entering into orbit, the dark count rate of the detectors is approximately 20 Hz. Because the detectors are exposed to radiation in the space environment, they are carefully shielded and cooled to −50 °C to reduce the dark counts to less than 150 Hz over a three-month period. A 3-nm narrowband filter is placed before the detectors to block stray light from the reflection of moonlight (maximum of about 350 Hz at full moon). We use time synchronization between the satellite and the ground (see Methods) to reliably extract four-photon coincidence counts within a time window of 3 ns.

To demonstrate that the quantum teleportation is universal, we test six input states in mutually unbiased bases on the Bloch sphere: $|H\rangle_1$, $|V\rangle_1$, $|+\rangle_1 = (|H\rangle_1 + |V\rangle_1)/\sqrt{2}$, $|-\rangle_1 = (|H\rangle_1 - |V\rangle_1)/\sqrt{2}$, $|R\rangle_1 = (|H\rangle_1 + i|V\rangle_1)/\sqrt{2}$ and $|L\rangle_1 = (|H\rangle_1 - i|V\rangle_1)/\sqrt{2}$. To evaluate the performance of the teleportation, we measure the fidelity of the teleported state $F = \mathrm{tr}(\hat{\rho}|\chi\rangle\langle\chi|)$, defined as the overlap between the ideal teleported state $|\chi\rangle$ and the measured density matrix $\hat{\rho}$. The teleported photon (photon 3) is measured using a polarization analyser that comprises a QWP, a HWP (both installed inside remotely controlled rotation mounts) and a PBS, followed by two single-photon detectors; the measurement projects photon 3 into either the ideal state $|\chi\rangle$ or its orthogonal state $|\chi\rangle^{\perp}$. Conditional on the detection of the trigger photon at the ground station and the two-photon double click after the Bell-state measurement, we register the photon counts of the teleported photon using the two-channel polarization analyser on the satellite, and record the two datasets. After applying 0 or π phase shift, depending on the outcome state ($|\phi^+\rangle_{12}$ or $|\phi^-\rangle_{12}$) of the Bell-state measurement, during post-processed of the data, we calculate the teleportation fidelity as the ratio of the correct four-photon coincidence counts and the overall four-photon events. Overall we obtain 911 four-photon counts in 32 orbits, with each orbit corresponding to 350 s of data collection. On the 32 different days, the orbits vary and so does the shortest distance between the satellite and the ground station (see Extended Data Table 1 for a summary). The fidelities of the teleportation state for the six input states are summarized in Fig. 3, yielding an average of $\overline{F} = 0.80 \pm 0.01$, sampling over the whole Bloch sphere. All data are reported without background subtraction.

The main sources of fidelity error are double-pair emission of SPDC (6%), partial photon distinguishability (10%), uplink polarization

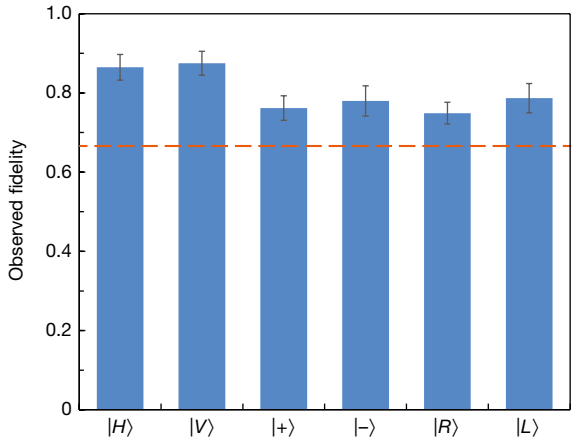

Figure 3 | Fidelity of the teleportation state for the six quantum states, with data taken for 32 orbits. Details of the date, the highest altitude angles and the ground-to-satellite distance for the 32 orbits are provided in Extended Data Table 1. All of the fidelities are well above the classical limit of 2/3 (dashed line). The error bars represent one standard deviation, calculated from Poissonian counting statistics of the raw detection events.

© 2017 Macmillan Publishers Limited, part of Springer Nature. All rights reserved.

distortion (3%) and background dark count (4%); see Methods for a more detailed analysis. Despite the photon loss and environmental noise, the measured fidelities of the teleportation state are all well above the classical limit of 2/3, which is defined as the optimal state-estimation fidelity on a single copy of a single-qubit system[14] that can be reached using a classical strategy without sharing entanglement as a resource. These results conclusively confirm the quantum nature of teleportation of a single qubit.

In summary, we have established a ground-to-satellite uplink over a distance of 500–1,400 km with loss of 41–52 dB and achieved reliable transfer of the superposition state of a single-photon qubit using quantum teleportation. As a comparison, using the same four-photon source and sending the teleported photon through a 1,200-km telecommunication fibre with loss of 0.2 dB km^{-1}, it would take 380 billion years (20 times the lifetime of the Universe) to witness one event, assuming the detectors have zero dark counts.

In this work, the entangled-photon source and the Bell-state measurement are performed at the same location on the ground. A next step towards real network connections is to realize long-distance entanglement distribution before the Bell-state measurement[10–12]. To this end, one approach is to develop an entangled-photon source with a long coherence time T_c and to reduce the arrival-time jitter T_j between independent photons such that $T_c > T_j$. Teleportation is not restricted to photons, but could also be used, for example, to transfer the quantum state of a fast-flying single photon to a long-lived matter qubit to achieve quantum memory at a distance[19–21]. Teleportation of a subsystem of an entangled pair is equivalent to the protocol of entanglement swapping[22–25], whereby two remote particles can become entangled without direct interaction. Teleportation of quantum logic gates, a key element in distributed quantum computing schemes, is also possible using shared multi-particle entangled states[5,6]. Given the rapid progress in long-lived quantum memories[26] and efficient light–matter interfaces[27], we expect that more sophisticated space-to-ground-scale teleportation will soon be realized, and will play a key part in a future distributed quantum internet.

Online Content Methods, along with any additional Extended Data display items and Source Data, are available in the online version of the paper; references unique to these sections appear only in the online paper.

Received 20 March; accepted 21 July 2017.
Published online 9 August 2017.

1. Wootters, W. K. & Zurek, W. H. A single quantum cannot be cloned. *Nature* **299,** 802–803 (1982).
2. Bennett, C. H. *et al.* Teleporting an unknown quantum state via dual classical and Einstein-Podolsky-Rosen channels. *Phys. Rev. Lett.* **70,** 1895–1899 (1993).
3. Briegel, H.-J., Dür, W., Cirac, J. I. & Zoller, P. Quantum repeaters: the role of imperfect local operations in quantum communication. *Phys. Rev. Lett.* **81,** 5932–5393 (1998).
4. Pan, J.-W. *et al.* Multiphoton entanglement and interferometry. *Rev. Mod. Phys.* **84,** 777–838 (2012).
5. Chuang, I. L. & Gottesman, D. Demonstrating the viability of universal quantum computation using teleportation and single-qubit operations. *Nature* **402,** 390–393 (1999).
6. Raussendorf, R. & Briegel, H. J. A one-way quantum computer. *Phys. Rev. Lett.* **86,** 5188–5191 (2001).
7. Bouwmeester, D. *et al.* Experimental quantum teleportation. *Nature* **390,** 575–579 (1997).
8. Yin, J. *et al.* Quantum teleportation and entanglement distribution over 100-kilometre free-space channels. *Nature* **488,** 185–188 (2012).
9. Ma, X.-S. *et al.* Quantum teleportation over 143 kilometres using active feed-forward. *Nature* **489,** 269–273 (2012).
10. Landry, O., van Houwelingen, J. A. W., Beveratos, A., Zbinden, H. & Gisin, N. Quantum teleportation over the Swisscom telecommunication network. *J. Opt. Soc. Am. B* **24,** 398–403 (2007).
11. Sun, Q.-C. *et al.* Quantum teleportation with independent sources and prior entanglement distribution over a network. *Nat. Photon.* **10,** 671–675 (2016).
12. Valivarthi, R. *et al.* Quantum teleportation across a metropolitan fibre network. *Nat. Photon.* **10,** 676–680 (2016).
13. Kimble, H. J. The quantum internet. *Nature* **453,** 1023–1030 (2008).
14. Massar, S. & Popescu, S. Optimal extraction of information from finite quantum ensembles. *Phys. Rev. Lett.* **74,** 1259–1263 (1995).
15. Kwiat, P. G. *et al.* New high-intensity source of polarization-entangled photon pairs. *Phys. Rev. Lett.* **75,** 4337–4341 (1995).
16. Chen, L.-K. *et al.* Observation of ten-photon entanglement using thin BiB_3O_6 crystals. *Optica* **4,** 77–83 (2017).
17. Pan, J.-W. & Zeilinger, A. Greenberger-Horne-Zeilinger-state analyzer. *Phys. Rev. A* **57,** 2208–2211 (1998).
18. Liao, S.-K. *et al.* Satellite-to-ground quantum key distribution. *Nature* **549,** https://doi.org/10.1038/nature23655 (2017).
19. Sherson, J. F. *et al.* Quantum teleportation between light and matter. *Nature* **443,** 557–560 (2006).
20. Chen, Y.-A. *et al.* Memory-built-in quantum teleportation with photonic and atomic qubits. *Nat. Phys.* **4,** 103–107 (2008).
21. Bussières, F. *et al.* Quantum teleportation from a telecom-wavelength photon to a solid-state quantum memory. *Nat. Photon.* **8,** 775–778 (2014).
22. Żukowski, M., Zeilinger, A., Horne, M. & Ekert, A. "Event-ready-detectors" Bell experiment via entanglement swapping. *Phys. Rev. Lett.* **71,** 4287–4290 (1993).
23. Pan, J.-W., Bouwmeester, D., Weinfurter, H. & Zeilinger, A. Experimental entanglement swapping: entangling photons that never interacted. *Phys. Rev. Lett.* **80,** 3891–3894 (1998).
24. Yuan, Z.-S. *et al.* Experimental demonstration of a BDCZ quantum repeater node. *Nature* **454,** 1098–1101 (2008).
25. Hensen, B. *et al.* Loophole-free Bell inequality violation using electron spins separated by 1.3 kilometres. *Nature* **526,** 682–686 (2015).
26. Zhong, M. *et al.* Optically addressable nuclear spins in a solid with a six-hour coherence time. *Nature* **517,** 177–180 (2015).
27. Yang, S.-J., Wang, X.-J., Bao, X.-H. & Pan, J.-W. An efficient quantum light–matter interface with sub-second lifetime. *Nat. Photon.* **10,** 381–384 (2016).

Acknowledgements We thank many colleagues at the National Space Science Center, National Astronomical Observatories and Xi'an Satellite Control Centre, especially B.-M. Xu, J. Li, J.-C. Gong, B. Chen, X.-J. Jiang and T. Xi, for their management and coordination. We thank T. Chen and Y.-H. Zhou from Ngari Observatory for their support during the experiment. This work was supported by the Strategic Priority Research Program on Space Science, the Chinese Academy of Sciences and National Natural Science Foundation of China.

Author Contributions C.-Z.P. and J.-W.P. conceived the research. C.-Z.P., J.-Y.W. and J.-W.P. designed the experiment. J.-G.R., X.P., H.-L.Y., J.Y., K.-X.Y., X.H., Y.-A.C., C.-Z.P. and J.-W.P. designed and developed the multi-photon sources. J.-G.R., H.-L.Y., K.-X.Y., X.H., J.L., H.-Y.W., C.-Z.P. and J.-W.P. designed and operated the telescopes. J.-G.R., L.Z., S.-K.L., J.Y., W.-Y.L., W.-Q.C., M.Y., Y.-W.K., Z.-P.H., S.W., L.L., D.-Q.L., R.S., Z.-C.Z., C.-Z.P., J.-Y.W. and J.-W.P. designed and developed the payloads on the satellite. H.-L.Y., L.Z., W.-Y.L., W.-Q.C. and P.S. developed the software. C.-Y.L., Y.-A.C., C.-Z.P. and J.-W.P. analysed the data and wrote the manuscript, with input from J.-G.R., P.X. and H.-L.Y. All the authors contributed to the data collection, discussed the results and reviewed the manuscript. J.-W.P. supervised the whole project.

Author Information Reprints and permissions information is available at www.nature.com/reprints. The authors declare no competing financial interests. Readers are welcome to comment on the online version of the paper. Publisher's note: Springer Nature remains neutral with regard to jurisdictional claims in published maps and institutional affiliations. Correspondence and requests for materials should be addressed to C.-Z.P. (pcz@ustc.edu.cn), J.-Y.W. (jywang@mail.sitp.ac.cn) or J.-W.P. (pan@ustc.edu.cn).

© 2017 Macmillan Publishers Limited, part of Springer Nature. All rights reserved.

METHODS

Ground observation. Ngari (Ali) prefecture in western Tibet, southwest of China, is one of the best astronomical observation sites in the world. It is considered to be competitive with high-altitude facilities at Mauna Kea, the Atacama Desert in Chile, and the Canary Islands[28–30].

The ground observation station for quantum teleportation is located at the top of Shiquanhe Daban Mountain in Ngari prefecture. The ground laboratory is built with coloured steel plates and thermal insulation materials (see Extended Data Fig. 3). The transmitting antennas are protected using a translational sliding roof, which is able to withstand winds of up to 20 m s^{-1}.

To improve experimental efficiency, we developed time division multiplexing technology, and an array of transmitting antennas is applied in the ground observation. In total three sets of antennas are used, two for daily use and the third as a backup. A corresponding photon source is linked to each antenna through a single-mode fibre.

Multi-photon sources. To increase the multi-photon count rate in our experiment we prepared three multi-photon teleportation modules (see Fig. 1b for one example), consecutively pumped by the same pulsed laser with 80-MHz repetition rate, and correspondingly three transmitting telescopes (Extended Data Fig. 4). The first and second modules were used in this work. In each module, the teleported single photons are coupled to a single-mode fibre and sent to a transmitting antenna. The two antennas used in this work are separated by 1.2 m, which is about six orders of magnitudes smaller than the separation between the antennas and the satellite (500–1400 km). This separation corresponds to a field angle of 0.8–2.4 μrad, much smaller than the system divergence (24–35 μrad); thus our system implements multiplexing naturally. The two multi-photon modules are delayed by an optical fibre for approximately 6 ns. Using time synchronization, the satellite can determine which module the received photons are from.

To improve the stability and portability of the modules we used an integrated structure design. A single four-photon source is integrated on a 4-cm-thick titanium base plate. Two CCDs with a pixel accuracy of 0.3 μm × 0.3 μm are used to monitor the pump-laser pointing. Two adjustable mirrors are used to correct the optical path.

Collinear and non-collinear BiBO crystals are positioned at the waist of the pump beam. The two crystals are closely mounted inside a specially designed bracket, with a spacing of less than 1 cm, well within the Rayleigh length (about 3 cm) of pump laser. The two crystals can be adjusted independently for optimal parametric down-conversion. This design reduces the size of the optical set-up such that it is easily accommodated in a base plate area of 460 mm × 510 mm (Extended Data Fig. 1). The pump laser is collimated and focused for the second module using two lenses.

We calibrate the fidelities of to-be-teleported photon, the entangled photon pairs and the teleported states on the ground. In the first module, the single-pair emission probability of the collinear SPDC is $\chi_{1c} \approx 0.08$ per laser pulse; the brightness of the six to-be-teleported states is $2.03 \times 10^6\,s^{-1}$, with a polarization-preparation fidelity of better than 99.8(0)%. For the entanglement source, the emission probability is $\chi_{1n} \approx 0.08$, the two-photon count rate is about $1 \times 10^6\,s^{-1}$ and its fidelity is 93.29(1)%. For the second module, the corresponding single-pair emission probabilities are $\chi_{2c} \approx 0.09$ and $\chi_{2n} \approx 0.11$. The brightness of six to-be-teleported states is $2.05 \times 10^6\,s^{-1}$, with a polarization preparation fidelity of better than 99.8(0)%. The two-photon count rate is about $1.15 \times 10^6\,s^{-1}$ and its fidelity is 90.19(2)%. The average overall system efficiency for each photon is about 32%, consisting of the optical and detection efficiencies, with the typical quantum efficiencies of single-photon detectors being about 70%. After the Bell-state measurement, the four-photon count rate is about 4,080 s^{-1} for the first module and 4,130 s^{-1} for the second module.

As shown in Fig. 1b, c, the teleported photon was guided through a 15-m single-mode fibre to the transmitting antenna, before being sent to the Micius satellite. Therefore, in principle, the outcome of the Bell-state measurement can arrive before the teleported photons. However, owing to the complexity of the overall design of the satellite's payloads and the experimental implementation, and as the first attempt of teleportation into space, we did not incorporate the active feedforward in this work. Instead, as a proof of principle, our experimental configuration allows us to post-process and analyse the data. Specifically, the Bell-state measurement will yield two outcomes, $|\phi\rangle_{12}^{+}$ and $|\phi\rangle_{12}^{-}$, corresponding to no operation and to a π phase shift, respectively. The two-detector configuration in the receiver satellite can simultaneously analyse these two cases. The fidelities of the six teleported states are listed in Extended Data Table 2.

Transmitting antennas and link losses. The transmitting antenna is composed mainly of three optical telescopes with 130-mm diameter (Extended Data Fig. 4). To improve the transmitting efficiency, a double off-axis parabolic structure is used in the telescopes. All of the optical components in the transmitting antenna are polarization-maintaining. The single-mode fibre changes the polarization state of transmitted photons. Here, we use a HWP and two QWPs to compensate the unitary polarization transformations caused in the single-mode fibres. An additional HWP is used to dynamically compensate the time-dependent polarization shift due to the relative motion of the satellite and the ground station. The polarization contrast of the whole system is maintained above 200:1. To keep the link fibre stationary while tracking the satellite, a periscope structure is used in the transmitting antenna, whereby the main body of the telescope remains stationary and the satellite is tracked via two rotatable mirrors.

The fast-steering mirror and the high-speed CCD constitute the fine-tracking system on the ground, which realizes pointing and tracking of the satellite with high accuracy. The tracking accuracy of the whole system is less than 3 μrad (1σ; Extended Data Fig. 2a, b). Two 671-nm beacon lasers (power of 2 W, divergence angle of 1.2 mrad) are installed on top of transmitting antennas 1 and 3 to track the satellite from the ground. Two 1,064-nm lasers (the second one is used as a backup) are installed on top of two of the transmitting antennas, and are used for time synchronization between the satellite and the ground station.

The locally tested beam divergence angle of the transmitting antenna when the beam does not pass through the atmosphere is 14 ± 1 μrad, as measured with a long-focal-length collimator (Extended Data Fig. 2c). If we consider the effect of the atmospheric seeing in Ngari, about 5 μrad, then the divergence angle is expected to be 15 μrad.

In the actual experimental configuration, the above-mentioned divergence angle was difficult to measure directly. The data presented in Extended Data Fig. 2d were measured indirectly by coupling the photons that were emitted from stars to the single-mode fibre and measuring the FOV of the intensity distribution as a function of fine-tracking scanning angle. Using such a method, many additional factors will affect the FOV as well as the expected 'pure' divergence angle (about 15 μrad), such as the mismatch between the diffraction spot size and the fibre core radius, the altitude angle of star, the precision of the tracking and changes in atmospheric environment, all of which can make the scanning result of the FOV larger. Here, the effective divergence angle was estimated from the measured FOV, which means that all of these additional effects were attributed to the equivalent divergence angle. The extracted equivalent divergence of 22 ± 3 μrad from Extended Data Fig. 2d is therefore larger than that expected purely from local testing and atmospheric seeing.

Finally, in relation to the fast-flying satellite, the beam divergence is tested by sending approximately 20 billion photons per second to the satellite from an attenuated laser, which are then collected by the satellite by varying the fine-tracking point. The intensity pattern that is obtained is elliptical, with a divergence of 24–35 μrad (Extended Data Fig. 2e).

The free-space link loss is composed of atmospheric transmittance and geometric loss. The optical transmittance is estimated to be 1.5 dB under usual weather conditions. The aperture of the receiving telescope in the satellite is 300 mm. The beam width when the beam arrives at the satellite will vary from about 10 m for the shortest uplink length (500 km) to 30 m for the longest (1,400 km), considering a divergence angle of 20 μrad (larger at a smaller altitude angle). The geometric loss is calculated to be 30.5–40 dB.

At the ground observatory, fibres and the optical elements in the transmitting antennas account for 1.5 dB of loss. At the satellite, the loss of coupling and the attenuation introduced by optical elements is 5.9 dB (including obscuration in the telescope). The loss from detection efficiency at the satellite is about 3 dB.

In total, the loss for the overall system therefore ranges from 42.4 dB to 51.9 dB under usual weather conditions. The best link loss is measured to be nearly 41 dB on good-weather days. The link loss is more than 50 dB when the length of the uplink is greater than 1,200 km.

Error analysis. There are many factors that influence the teleportation fidelity, such as double-pair emission of SPDC, partial photon distinguishability, uplink polarization distortion and background dark counts.

To be specific, for the collinear BiBO crystal in our system, the quantum state of SPDC photons (photon 1 and the trigger (T) photon) is

$$|\Psi\rangle_{1T} = |\mathrm{vac}\rangle + \sqrt{\chi}(\hat{a}_1^{\dagger}\hat{a}_T^{\dagger})|\mathrm{vac}\rangle + \frac{\chi}{2}(\hat{a}_1^{\dagger}\hat{a}_T^{\dagger})^2|\mathrm{vac}\rangle$$

Here, the higher-order terms are neglected, χ is the single photon-pair emission probability, $|\mathrm{vac}\rangle$ is the vacuum state and $\hat{a}^{\dagger}$ is the creation operator. From this equation, we find that the probability of the double-pair emission is about χ^2. Similarly, this conclusion can also be derived from the Einstein–Podolsky–Rosen source. Owing to the limited working time of the satellite, we give priority to improving the brightness and stability in the entanglement source modules. As shown in Extended Data Table 2, the fidelity of state $|H\rangle$ is higher than that of $|+\rangle$. This is because $|H\rangle$ is affected only by the noise from double-pair emission, whereas $|+\rangle$ is also affected by partial distinguishability of independent photons that overlap on the PBS.

© 2017 Macmillan Publishers Limited, part of Springer Nature. All rights reserved.

The coincidence count can be generated between the dark counts from the satellite detectors and the threefold coincident counts from the ground station, which we refer to as 'accidental coincidence counts'. To ensure a high signal-to-noise ratio, we avoided five nights close to full moon, during which there would be greater background noise. In addition, to ensure reasonably high link efficiencies, we selected only the orbits for which the highest altitude angle was more than 20° (which occurs with >96% probability).

Time synchronization. On the transmitting antenna we used a 1,064-nm pulsed laser to synchronize the time of the quantum signal between the ground station and the satellite. This Q-switched laser produces short pulses (pulse width of about 800 ps) with a repetition frequency of 10 kHz. After passing through the ground-to-satellite link, these optical pulses are coupled to the photo detector on the satellite, and then recorded in the time-to-digital convertor (TDC). At the ground station, the laser also synchronously produces a synchronized electrical signal, the time information of which is recorded in the TDC at the ground station. In the local test, the jitter between the local electrical signal and the transmitted optical signal is around 100 ps.

In previous ground-based experiments, a TDC also records one pulse-per-second (PPS) signal from a global positioning system (GPS) to assist with matching the synchronized optical signals. However, owing to the high-speed motion of the satellite, the distance information of the ground-to-satellite link needs to be compensated in the calculation. In the experiment, the synchronization error is about 0.7 ns (Extended Data Fig. 5). As mentioned previously, we use three transmitting antennas to simultaneously transmit quantum signals to the satellite, which further increased the complexity of synchronization. When more than one transmitting antenna sends signal photons to the satellite at the same time, the distance between different antennas and the satellite will be slightly different. The maximum difference is close to the distance between antennas (1.2 m). There is no signal crosstalk in our scheme.

To improve the signal-to-noise ratio during the satellite-to-ground synchronization, we need to avoid the uncertainty of quantum signal transmission to reduce the gate width. For the antenna on which the synchronous laser is installed, the time delay between the quantum signal link and the synchronous optical link is almost the zero; the quantum signal from the antenna without the synchronous laser is compensated by a time delay, which is calculated from the orbit data. The latter case is then equivalent to the former.

Data availability. The data that support the findings of this study are available from the corresponding authors on reasonable request.

28. Stone, R. World-class observatory rising on 'Roof of the World'. *Science* **337,** 1156–1157 (2012).
29. Yao, Y. *et al.* Site characterization studies in high plateau of Tibet. *Proc. SPIE* **8444,** 84441K (2012).
30. Wang, H., Yao, Y., Liu, L., Qian, X. & Yin, J. Optical turbulence characterization by WRF model above Ali, Tibet. *J. Phys. Conf. Ser.* **595,** 012037 (2015).

© 2017 Macmillan Publishers Limited, part of Springer Nature. All rights reserved.

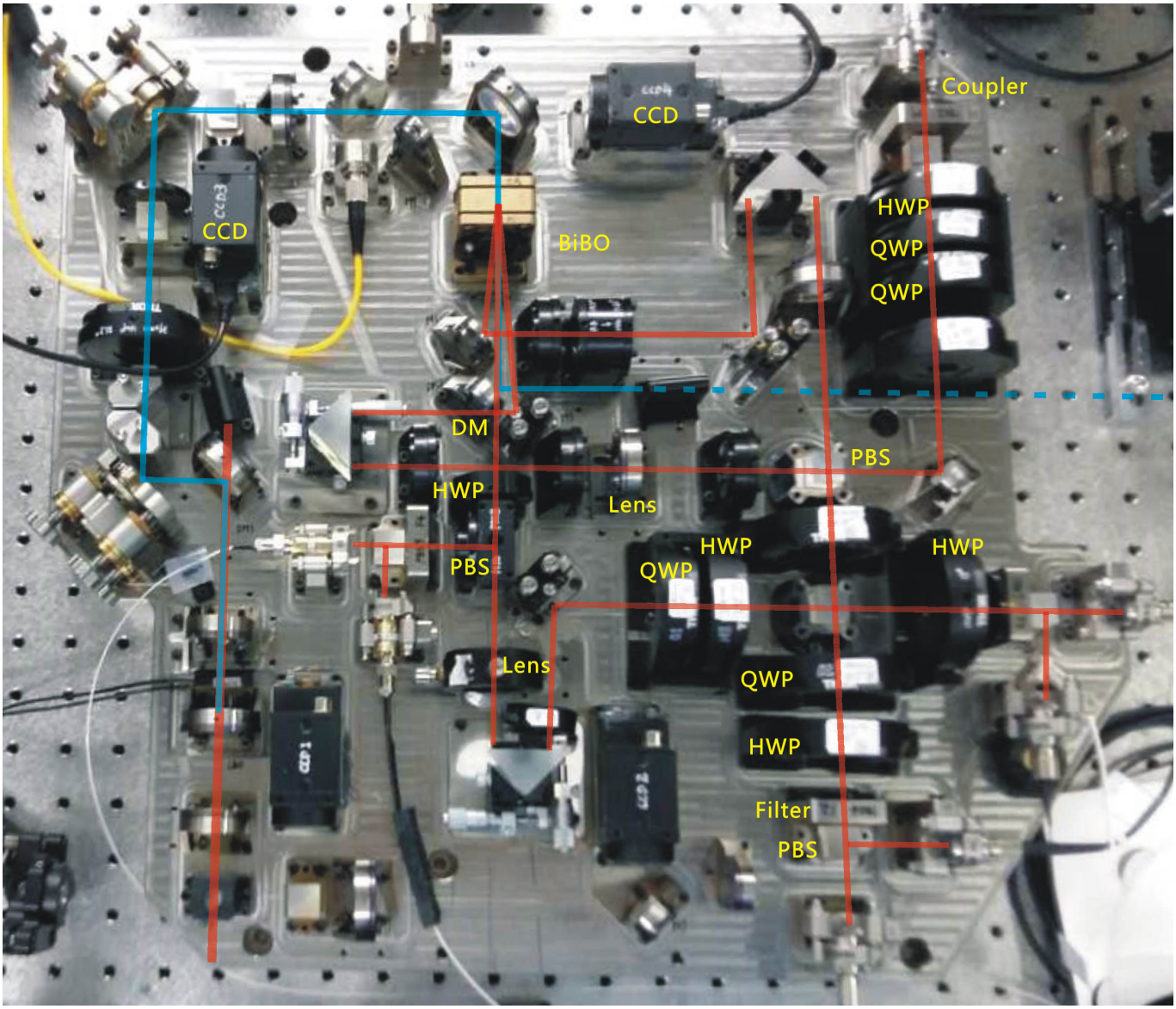

Extended Data Figure 1 | Structure of the first module. The only difference from the other two modules is that this module contains a second-harmonic-generation device to generate the 390-nm-wavelength pump laser (blue solid line). In working conditions, the light trap that collects the pump laser will be replaced by a lens, and the laser will be sent to the next module (blue dotted line). 780-nm-wavelength light is indicated by the red line. DM, dichroic mirror; HWP, half-wave plate; QWP, quarter-wave plate; PBS, polarizing beam splitter.

© 2017 Macmillan Publishers Limited, part of Springer Nature. All rights reserved.

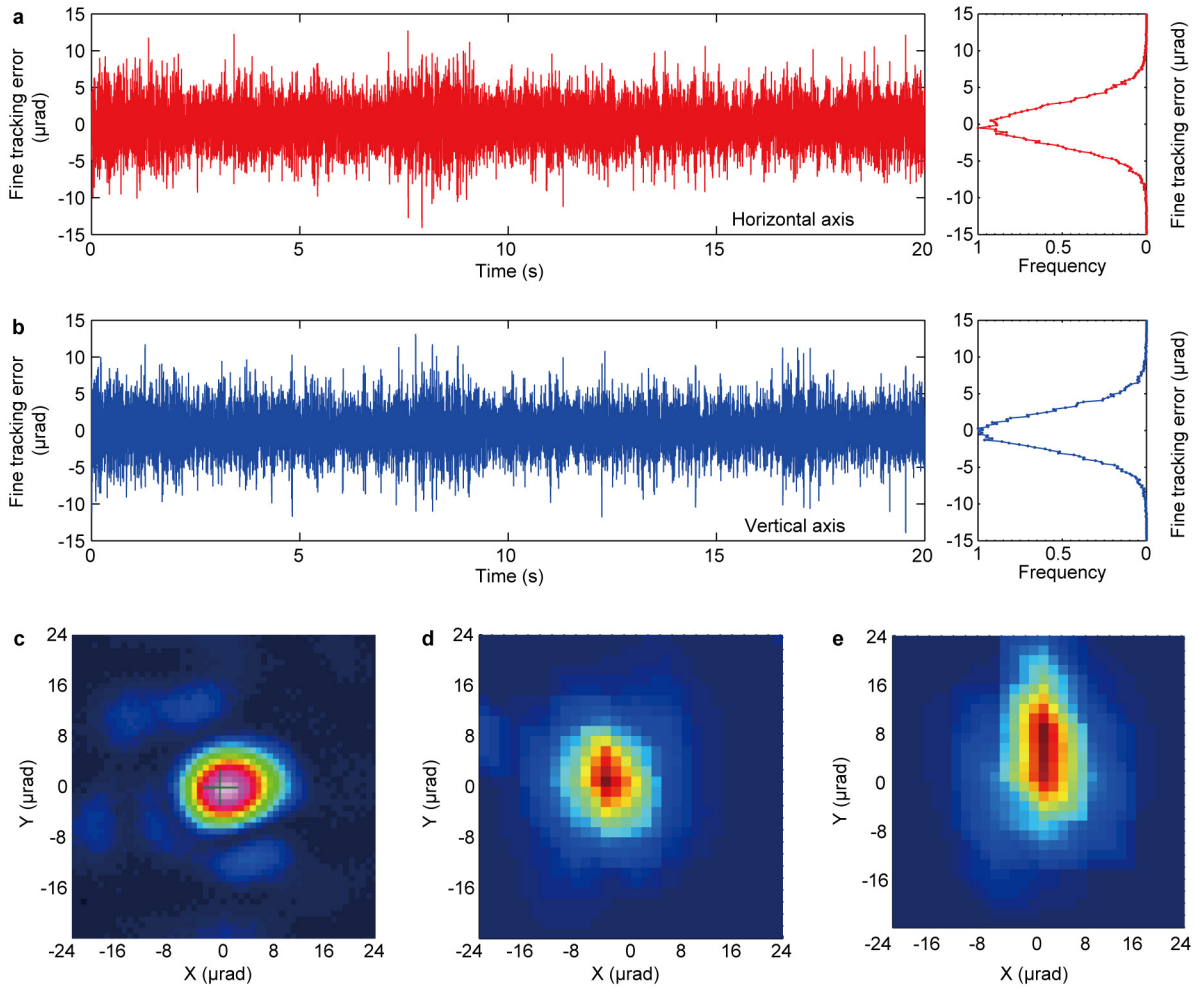

Extended Data Figure 2 | Establishing a reliable ground-to-satellite link for teleportation. a, **b**, Performance of the APT system on the *X* (horizontal; **a**) and *Y* (vertical; **b**) axes. The left panels show real-time tracking errors that are read out from the camera with a sampling rate of 2 kHz. The right panels show frequency counts of the tracking error, which is used to extract a full-width at half-maximum (FWHM) of 6.5 μrad (*X* axis) and 6.3 μrad (*Y* axis). **c**–**e**, Tests of beam diffraction and wandering. **c**, Divergence angle from a local test. The image is obtained by using a CCD camera set at the focal plane at a 7-m local length collimator. The beam diameter is measured to be approximately 94 μm. The divergence angle is approximately 14 ± 1 μrad. **d**, Intensity profile of photons from a distant star coupled to the single-mode fibre through the telescope. The effective divergence angle estimated from the measured FOV of the intensity distribution is approximately 22 ± 3 μrad. **e**, The intensity pattern obtained by the satellite's CCD camera is elliptical, with a divergence of 24–35 μrad.

© 2017 Macmillan Publishers Limited, part of Springer Nature. All rights reserved.

Extended Data Figure 3 | Aerial photograph of the teleportation ground station. Multi-photon sources are prepared in the laboratory on the first floor. Three transmitting antennas are set on a high cement pier and arranged at the same latitude.

© 2017 Macmillan Publishers Limited, part of Springer Nature. All rights reserved.

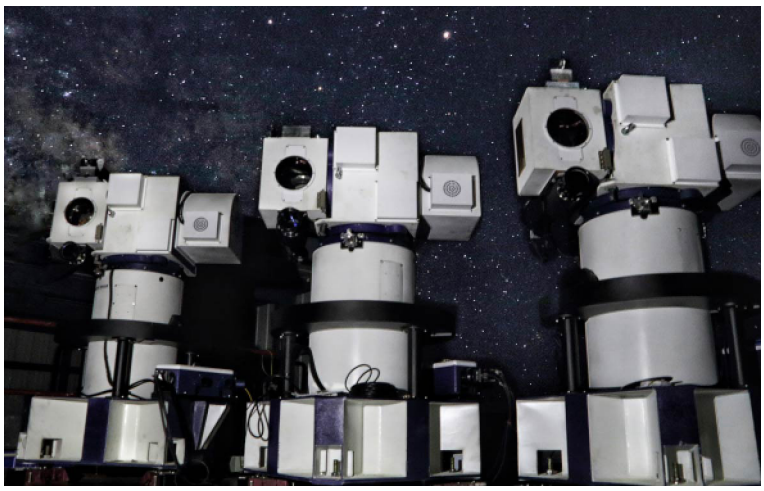

Extended Data Figure 4 | Photograph of three transmitting antennas at night. The ground station in Ngari, Tibet, is one of the world's best protected dark-night zones. Three transmitting antennas are placed side by side on a platform. Quantum signals generated from the laboratory on the first floor are transmitted to the three telescopes. The beacon lasers and the synchronization laser are arranged on top of the transmitting antennas.

© 2017 Macmillan Publishers Limited, part of Springer Nature. All rights reserved.

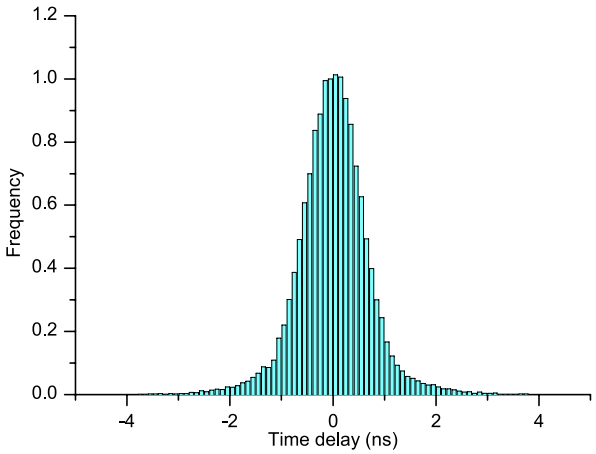

Extended Data Figure 5 | Histogram of the time difference in time synchronization. The histogram gives statistical information about the time-difference distribution of the synchronization detections at the ground and the satellite. The flight time from the ground to the satellite changes from 1.6 ms to 5 ms. A clear peak is evident in the time difference between synchronization signals after subtracting the flight time and comparing with neighbouring signals. One standard error of the time difference is about 0.7 ns. The FWHM of the histogram is less than 2 ns. The coincidence window is therefore set to 3 ns for a better signal-to-noise ratio.

© 2017 Macmillan Publishers Limited, part of Springer Nature. All rights reserved.

Extended Data Table 1 | Statistics of the 32 orbits used for the data collection of quantum teleportation

Date	Highest altitude angle	Shortest distance (km)	collected 4-photon counts
17/09/2016	53.7°	590	29
19/09/2016	24.3°	1022	8
25/09/2016	76.0°	499	59
28/09/2016	26.3°	971	9
30/09/2016	69.9°	515	54
13/10/2016	86.8°	494	60
14/10/2016	40.0°	732	27
17/10/2016	68.6°	529	34
21/10/2016	49.8°	635	18
5/11/2016	41.1°	730	13
8/11/2016	68.4°	537	24
10/11/2016	26.9°	984	18
13/11/2016	75.4°	517	14
16/11/2016	37.9°	771	16
17/11/2016	81.4°	506	30
18/11/2016	46.3°	670	22
20/11/2016	29.2°	926	9
21/11/2016	60.5°	567	23
22/11/2016	62.4°	557	35
26/11/2016	83.7°	499	25
27/11/2016	38.3°	757	25
1/12/2016	50.8°	622	28
4/12/2016	54.6°	593	64
5/12/2016	68.3°	526	59
7/12/2016	21.0°	1127	14
8/12/2016	41.1°	723	28
17/12/2016	50.5°	615	19
18/12/2016	73.3°	504	34
19/12/2016	33.3°	820	8
23/12/2016	43.5°	676	23
27/12/2016	58.1°	561	51
30/12/2016	47.3°	639	31

The lowest altitude angle is always 14.5°, at which the satellite-to-ground distance is 1,400 km.

© 2017 Macmillan Publishers Limited, part of Springer Nature. All rights reserved.

Extended Data Table 2 | Observed fidelities of the teleported states in ground tests

States	Fidelity (%) First module	Fidelity (%) Second module
$\|H\rangle$	92.54 (44)	94.42 (43)
$\|V\rangle$	93.93 (36)	90.61 (45)
$\|+\rangle$	80.07 (63)	77.13 (66)
$\|-\rangle$	80.22 (63)	77.32 (64)
$\|R\rangle$	80.09 (61)	77.27 (66)
$\|L\rangle$	79.97 (62)	76.79 (68)

The error in parentheses is one standard deviation, calculated from Poissonian counting statistics.

© 2017 Macmillan Publishers Limited, part of Springer Nature. All rights reserved.